Computational fluid dynamics modelling of large-scale bubble columns: from the mono-dispersed to the pure heterogeneous flow regime

Journal of Physics: Conference Series **2766** (2024) 012059 doi:10.1088/1742-6596/2766/1/012059

Computational fluid dynamics modelling of large-scale bubble columns: from the mono-dispersed to the pure heterogeneous flow regime

Nicolò Varallo, Riccardo Mereu, Giorgio Besagni and Fabio Inzoli
Politecnico di Milano, Department of Energy, via Lambruschini 4a, 21156, Milano, Italy
E-mail: nicolo.varallo@polimi.it

Abstract. This study proposes a CFD model to simulate large-scale bubble columns operating in different flow regimes. Transient 3-D simulations were performed employing a commercial code (ANSYS Fluent), and the numerical results were compared with available experimental data. The superficial gas velocity ranges between 0.0037 m/s and 0.2 m/s, covering both the mono-dispersed and pure-heterogenous flow regimes, where bubbles coalescence and breakup were modelled. The results have been critically analysed, and the discrepancies between the numerical and experimental results have been deeply commented on, setting the stage for future improvements.

1. Introduction

Bubble columns are gas-liquid reactors widely used in many industrial applications due to their several advantages. They are characterized by a simple design and operation due to the absence of moving parts, low operating costs, and excellent heat and mass transfer between the phases [1]. Despite the simple column layout, bubble columns fluid dynamics is extremely complex due to the interactions between the continuous liquid and dispersed gas phases, manifesting in the prevailing flow regime.

When dealing with industrial applications, large-scale bubble columns must be considered. The fluid dynamics definition of large-scale bubble columns is related to the absence of the slug flow regime resulting from Rayleigh-Taylor instabilities. These instabilities can be quantified at the reactor scale by comparing the non-dimensional diameter (D_H^*) with a critical diameter ($D_{H,cr}^*$) [2]:

$$D_H^* = \frac{D_H}{\sqrt{\sigma / g(\rho_L - \rho_G)}} > D_{H,cr}^* \approx 52 \tag{1}$$

In equation (1), D_H is the column hydraulic diameter, σ is the gas-liquid surface tension, g is the acceleration due to gravity, ρ_L is the liquid phase density, and ρ_G is the gas phase density. A bubble column is classified as a large-scale reactor if D_H^* exceeds $D_{H,cr}^* \approx 52$ (i.e. $D_H \approx 0.15$ m at ambient conditions).

Increasing the gas flow rate, six flow regimes can be encountered in large-scale bubble columns [3]: (1) mono-dispersed homogeneous flow regime, (2) poly-dispersed homogeneous flow regime, (3) transition flow regime without coalescence-induced structures, (4) transition

flow regime with coalescence-induced structures, (5) pseudo-heterogeneous flow regime, and (6) pure heterogeneous flow regime.

Understanding the fluid dynamics, the interactions between the phases, and the transport phenomena involved is essential to support bubble column design and scale-up. In this regard, there is growing attention on computational fluid dynamics (CFD) to predict and understand the multiphase flow field in bubble columns ([4]; [5]; [6]). Indeed, the correct estimation of global (global gas holdup) and local (local gas holdup and bubble size distribution) flow properties is essential for designing, operating, and scaling up bubble columns [7].

This paper presents a numerical model for simulating bubble columns operating in different flow regimes. In particular, different lift coefficient correlations are compared and different strategies to model the dispersed phase are considered: (i) the fixed mono-dispersed approach for simulating the mono-dispersed homogeneous flow regime, (ii) the fixed poly-dispersed approach for simulating the poly-dispersed homogeneous flow regime, and (iii) the poly-dispersed approach with bubble coalescence and breakup for simulating the pure-heterogeneous flow regime.

The paper is organized as follows. The experimental benchmark used for the model validation is briefly presented in section 2. The numerical model is described in section 3, and the results are presented in section 4. Finally, conclusions are drawn, and avenues for future studies are proposed.

2. The experimental benchmark

The model validation was performed by comparing the numerical results with available experimental data from [3]. The experimental facility is a non-pressurized bubble column with an inner diameter of 0.24 m and a height of 5.3 m. Different spargers were tested: perforated plate sparger with 581 holes of 0.5 mm, needle sparger with 581 needles of 0.5 mm diameter, and spider sparger with 6 arms having holes ranging between 2 mm and 4 mm.

Measurement of the bed expansion (the height of the liquid free surface when air flows in the column) allowed the evaluation of the global gas holdup, and a double-fiber optical probe system (manufactured by RBI) was used to measure the local fluid dynamics properties (i.e., local gas holdup). The optical probe was inserted, via an access port, into the flow at an axial position of 1.9 m from the sparger. Finally, image analysis was performed to obtain the bubble size distribution.

3. The numerical model

3.1. The governing equations

The numerical simulations presented were performed considering the two-fluid Eulerian–Eulerian approach, which is based on ensemble-averaged mass and momentum transport equations for each phase. For an isothermal flow without mass transfer, the unsteady Reynolds averaged Navier-Stokes equations for the generic k-th phase are:

$$\frac{\partial}{\partial t}(\alpha_k \rho_k) + \nabla \cdot (\alpha_k \rho_k \vec{u}_k) = 0 \tag{2}$$

$$\frac{\partial}{\partial t}(\alpha_k \rho_k \vec{u}_k) + \nabla \cdot (\alpha_k \rho_k \vec{u}_k \vec{u}_k) = -\alpha_k \nabla p + \nabla \cdot (\alpha_k \bar{\tau}_k) + \alpha_k \rho_k \vec{g} + \vec{M}_{I,k} \tag{3}$$

The right-hand side term of equation (3) represents the pressure gradient, the stresses (Reynolds and viscous), the body forces, and the interfacial momentum exchanges between the phases, which comprises several physical mechanisms, namely drag, lift, turbulent dispersion, wall lubrication, and virtual mass forces:

$$\vec{M}_{I,k} = \vec{F}_{D,k} + \vec{F}_{L,k} + \vec{F}_{TD,k} + \vec{F}_{WL,k} + \vec{F}_{VM,k} \tag{4}$$

A summary of the closure models for the momentum exchange between the phases used in this study is presented in table 1.

Table 1. Summary of the closure models for the interfacial momentum exchange used in this study. It has to be pointed out that only the drag and lift forces are considered for the pure-heterogeneous flow regime case.

Interfacial force	**Model**
Drag	Tomiyama et al. (1998) [8]
Lift	Tomiyama et al. (2002) [9], Ziegenhein et al. (2018) [10], Hessenkemper et al. (2021) [11]
Turbulent dispersion	Burns et al. (2004) [12]
Wall lubrication	Antal et al. (1991) [13]
Virtual mass	Not considered

3.2. Turbulence modelling

The two-equation $k-\omega$ SST model was used for the continuous phase, as suggested in [14]. On the contrary, due to the small gas density, turbulence was neglected in the dispersed gas phase [15]. In the present study, bubble-induced turbulence was not considered.

3.3. Dispersed phase modelling

When dealing with the dispersed phase modelling, three approaches can be used:

- **Fixed mono-dispersed approach**. This approach concerns the mono-dispersed homogeneous flow regime. The bubble size distribution is below the critical diameter for the change in the sign of the lift force, and only small bubbles are considered. In the fixed mono-dispersed approach, the dispersed phase is modelled using a single gas phase, and the bubble diameter is assigned based on the experimental value.
- **Fixed poly-dispersed approach**. This approach concerns the poly-dispersed homogeneous flow regime. This study implements two bubble classes to consider the different dynamics of small and large bubbles resulting from a different lift force.
- **Poly-dispersed approach with bubble coalescence and break-up**. This approach concerns the pure-heterogeneous flow regime, where bubble coalescence and breakup cannot be neglected. The CFD model is coupled with a population balance model, and closure relations for bubble coalescence and breakup are required. In this study, nine bubble classes were considered. Bubble coalescence and breakup were modelled considering the kernels of Wang et al. [16] and Lehr et al. [17], respectively. The inlet bubble size was assumed to have a log-normal distribution with a constant variance about the mean value. The Cao et al. [18] correlation was used to calculate the inlet mean bubble size, whereas the variance was determined from the experimental data.

Table 2 and figure 1, figure 2, and figure 3 present the cases considered in this study.

Table 2. Cases studied.

Case	Sparger	Flow regime	Dispersed phase modelling approach
C1	Needle	Mono-dispersed	Fixed mono-dispersed
C2	Perforated plate	Poly-dispersed	Fixed poly-dispersed
C3	Spider	Pure-heterogeneous	Poly-dispersed with bubble coalescence and breakup

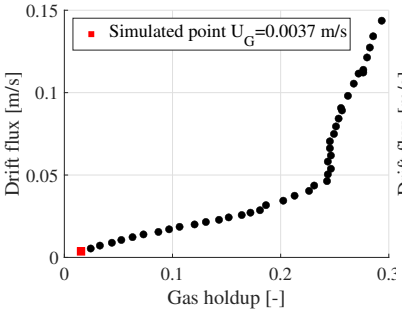

Figure 1. Case C1.

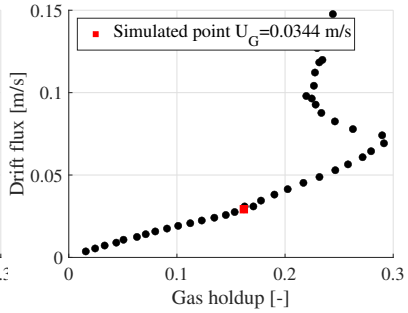

Figure 2. Case C2.

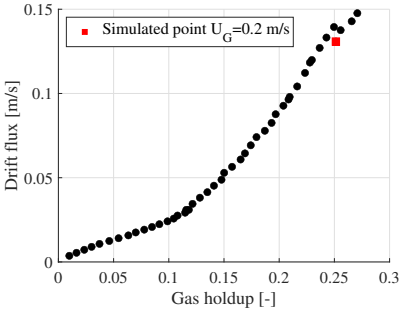

Figure 3. Case C3.

3.4. Numerical settings and boundary conditions

The transient simulations were performed using the commercial code ANSYS Fluent on a 3-D cylindrical domain. The bubble column was discretized using a hexahedral mesh concerning the column equipped with the perforated plate and needle spargers. Instead, a polyhedral mesh was used for the column equipped with the spider sparger since it was modelled considering its fully 3-D structure without any simplification. A mesh sensitivity analysis was performed to ensure the results are independent of the mesh size. In particular, three meshes, namely coarse, medium, and fine, were tested for both geometries. The mesh sensitivity results are shown in table 3 and table 4. The medium mesh was used for both geometries. In addition, the mesh size decreases moving towards the column wall to ensure $y^+ < 5$.

The results were averaged over 60 seconds of flow time to guarantee the independence of the initial transient. The time step size was set equal to 0.005 seconds, with a Courant-Friedrichs-Lewy number lower than 1. The Phase-Couple SIMPLE (PC-SIMPLE) algorithm was used for the pressure-velocity coupling. A second-order bounded Euler implicit scheme was used for the temporal discretization. The least squares cell-based formulation and the PRESTO! discretization schemes were considered for the spatial representation of gradients and pressure, respectively. In bubble columns, high-order schemes are required to describe the transient nature of the flow. Thus, the QUICK method (third-order accuracy) was implemented for both momentum and volume fraction equations. The second-order upwind scheme was chosen for the turbulent quantities instead.

A uniform inlet was used to model the gas sparger for case studies C1 and C2, and the gas velocity was imposed at the column inlet. Concerning case study C3, the spider sparger was modelled with its fully 3-D structure, and a velocity boundary condition was imposed at each hole. Since the column was operated in the batch mode the water flow rate was zero at the inlet section. The turbulent quantities were set according to Kawase and Moo-Young [19]. A degassing boundary condition was assigned to the column outlet.

The phases properties were evaluated at ambient temperature and pressure.

Table 3. Mesh sensitivity study: uniform inlet case.

Mesh	Number of elements	ε_G [-]
Coarse	170 000	0.0149
Medium	270 000	0.0154
Fine	392 000	0.0154

Table 4. Mesh sensitivity study: spider sparger case.

Mesh	Number of elements	ε_G [-]
Coarse	230 000	0.2382
Medium	313 000	0.2496
Fine	436 000	0.2498

4. Results

This section compares the global time-averaged gas holdup (ε_G) and local time-averaged gas holdup profiles with the experimental data.

The numerical model allows a correct estimation of the global gas holdup, with a relative error of less than 3% for all the cases studied (table 5).

The results concerning case study C3 were obtained by modifying the Tomiyama drag coefficient with a swarm factor [20] to include the influence of bubble clustering in the model. Indeed, the drag coefficient alone was not sufficient to capture the flow dynamics and a largely overestimated value of the global gas holdup was computed (relative error larger than 100 %).

Table 5. Comparison between the experimental and calculated global gas holdup. The relative error has been compute as $e_{\%} = |y_{\mathrm{EXP}} - y_{\mathrm{CFD}}|/y_{\mathrm{EXP}} \cdot 100$.

Case	Lift model	$\varepsilon_{G,\mathrm{EXP}}$ [-]	$\varepsilon_{G,\mathrm{CFD}}$ [-]	$e_{\%}$ [%]
C1	Tomiyama	0.0154	0.0155	0.649
C1	Ziegenhein	0.0154	0.0155	0.649
C2	Tomiyama	0.1626	0.1585	2.523
C2	Ziegenhein	0.1626	0.1592	2.079
C2	Hessenkemper	0.1626	0.1587	2.392
C3	Ziegenhein	0.2496	0.2463	1.338

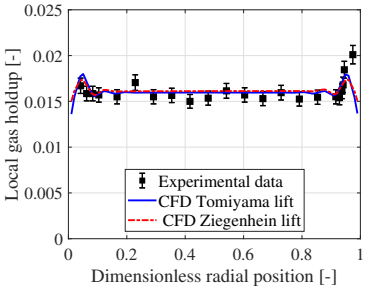

Figure 4. Case C1.

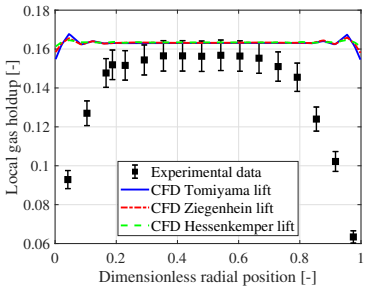

Figure 5. Case C2.

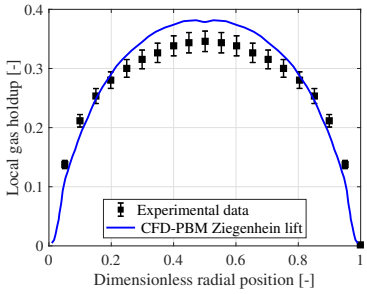

Figure 6. Case C3.

Moving to the local gas holdup profiles, the results are presented in figure 4, figure 5, and figure 6. Starting from case study C1, which deals with the mono-dispersed homogeneous flow regime, the numerical results agree with the experimental data in the column centre and near the wall. Figure 4 compares the Tomiyama and the Ziegenhein lift coefficient models, which provide the same results. Indeed, the two profiles are superimposed, and the same was found

with the Hessenkemper lift model, whose results have not been reported in the figure for the sake of clarity.

Moving to case study C2, which deals with the poly-dispersed homogeneous flow regime, from figure 5, it is evident that the numerical model fails to predict the near-wall local gas holdup profile. In addition, the numerical profiles are completely flat, even if large bubbles have been included in the model. The reason for the wrong prediction of the local gas holdup profile can be explained either by a too-weak lift force concerning the large bubbles or by a too-strong turbulent dispersion force. Indeed, the turbulent dispersion force is proportional to the local void fraction gradient, and it redistributes the bubbles in the lateral direction from regions with high bubble concentrations to regions with low bubble concentrations. Consequently, it modulates peaks of small bubbles near the wall pipe and spreads out large bubbles. The different lift coefficient correlations provide identical results at the column centre, with the Hessenkemper and Ziegenhein models that give less pronounced wall peaks concerning the Tomiyama lift model.

Finally, moving to case study C3, which deals with the pure-heterogeneous flow regime, the numerical model provides satisfying results. The numerical profile (figure 6) is centre-picked, overestimating the gas holdup at the column centre. It has to be pointed out that the turbulent dispersion force was not included in the model, and consequently, its spreading effect on large bubbles was not considered.

5. Conclusions

This study proposed a numerical model to simulate large-scale bubble columns operating in the mono-dispersed homogeneous, poly-dispersed homogeneous, and pure heterogeneous flow regimes. The calculated global gas holdup agrees with the experimental data, with a relative error of less than 3 % for all the cases considered. Satisfying results concerning local gas holdup profiles are obtained in the mono-dispersed homogeneous and pure heterogeneous flow regimes. However, the proposed numerical model fails to predict the near-wall local holdup in the poly-dispersed homogeneous flow regime.

Future studies should investigate the influence of the forces acting in the lateral direction on bubble motion since they are fundamental in predicting physical local holdup profiles.

References

[1] Kantarci N, Borak F and Ulgen K O 2005 *Process Biochem.* **20** 2263-2283.
[2] Besagni G, Di Pasquali A, Gallazzini L, Gottardi E, Colombo L P M and Inzoli F 2017 *Int. J. Multiph. Flow* **94** 53-78.
[3] Besagni G 2021 *Int. J. Multiph. Flow* **135** 103510.
[4] Rzehak R, Ziegenhein T, Kriebitzcsh S, Krepper E and Lucas D 2017 *Chem. Eng. Sci.* **157** 147-158.
[5] Guan X and Yang N 2021 *Chem. Eng. Sci.* **243** 116758.
[6] Khan H, Kováts P, Zähringer K and Rzehak R 2024 *Chem. Eng. Sci.* **285** 119503.
[7] Shaikh A and Al-Dahhan M 2013 *Ind. Eng. Chem. Res.* **52** 8091-8108.
[8] Tomiyama A, Sou A, Kanami N and Sakaguchi T 1995 *In: Proc. 2nd Int. Conf. on Multiphase Flow ICMF.*
[9] Tomiyama A, Tamai H, Zun I and Hosokawa S 2002 *Chem. Eng. Sci.* **57** 1849-1858.
[10] Ziegenhein T, Tomiyama A and Lucas D 2018 *Int. J. Multiph. Flow* **108** 11-24.
[11] Hessenkemper H, Ziegenhein T, Rzehak R, Lucas D and Tomiyama A 2021 *Int. J. Multiph. Flow* **138** 103587.
[12] Burns A D, Frank T, Hamill I and Shi J M 2004 *In: Proc. 5th Int. Conf. on Multiphase Flow ICMF.*
[13] Antal S P, Lahey Jr R T and Flaherty J E 1991 *Int. J. Multiph. Flow* **17** 635-652.
[14] Ziegenhein T, Rzehak R and Lucas D 2015 *Chem. Eng. Sci.* **122** 1-13.
[15] Rzehak R and Krepper E 2013 *Nucl. Eng. Des.* **265** 701-711.
[16] Wang T, Wang J and Jin Y 2005 *In: Proc. 7th Int. Conf. on Gas-Liquid and Gas-Liquid-Solid Reactor Engineering.*
[17] Lehr F, Milles M and Mewes D 2002 *AIChE J.* **48** 2426-2443.
[18] Cao C, Zhao L, Xu D, Geng Q and Guo Q 2009 *Ind. Eng. Chem. Res.***48** 5824-5832.
[19] Kawase C and Moo-Young M 1989 *The Chemical Engineering Journal* **40** 55-58.
[20] Gemello L, Cappello V, Auigier F, Marchisio D and Plais C 2018 *Chem. Eng. Res. Des.* **136** 846-858.